Quarkonium Production and Suppression at the LHC

R. Vogt

Lawrence Livermore National Laboratory, Livermore, CA
Physics Department, University of California, Davis, CA

Outline

- Baseline Nuclear Effects on Quarkonium Production
  - Rapidity and p_T Distributions
  - Initial-State Shadowing
  - Final-State Absorption
  - Comparison to RHIC d+Au and $A+A$ Data
  - Cold Matter Effects on J/ψ and Υ Production at the LHC
- Quarkonium Suppression by Plasma Screening
  - Survival Probability as a Function of p_T
  - ψ'/ψ and Υ'/Υ as a function of p_T

J/ψ and Υ NLO CEM Cross Sections

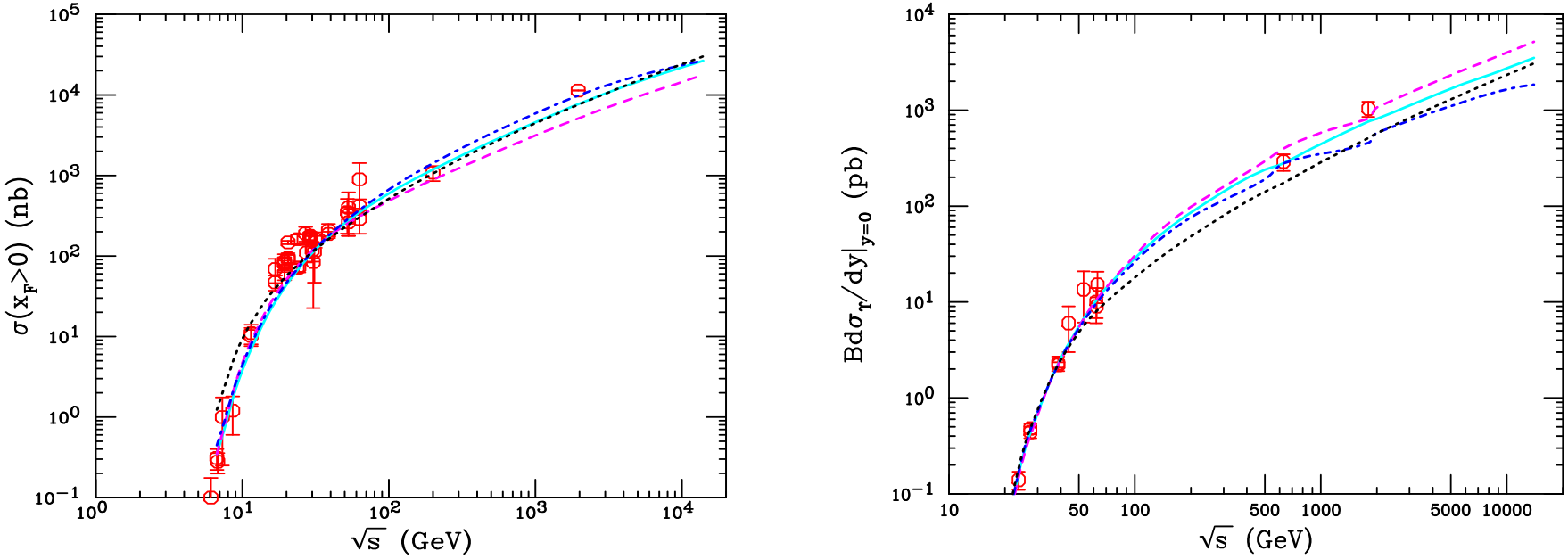

Figure 1: (Left) The NLO J/ψ forward cross sections. The solid curve employs the MRST HO distributions with $m = 1.2$ GeV $\mu/m_T = 2$, the dashed, MRST HO with $m = 1.4$ GeV $\mu/m_T = 1$, the dot-dashed, CTEQ 5M with $m = 1.2$ GeV $\mu/m_T = 2$, and the dotted, GRV 98 HO with $m = 1.3$ GeV $\mu/m_T = 1$. (Right) Inclusive Υ production data, combined from all three S states, and compared to NLO CEM calculations. The solid curve employs the MRST HO distributions with $m = 4.75$ GeV $\mu/m_T = 1$, the dashed, $m = 4.5$ GeV $\mu/m_T = 0.5$, the dot-dashed, $m = 5$ GeV $\mu/m_T = 2$, and the dotted, GRV 98 HO with $m = 4.75$ GeV $\mu/m_T = 1$.

.

Predictions of Quarkonia Rapidity Spectra at LHC

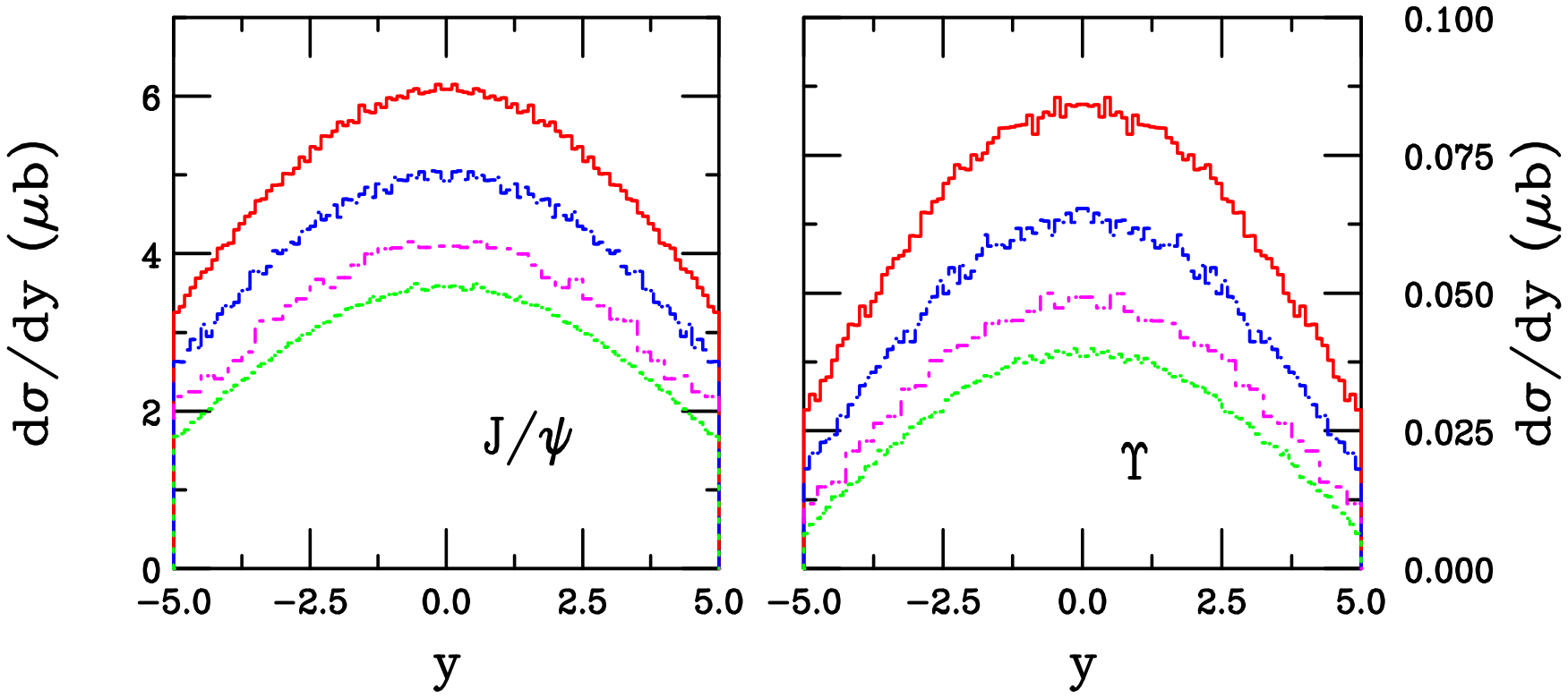

Figure 2: The inclusive J/ψ (left) and Υ (right) rapidity distributions, calculated for the GRV98 parton densities (cases $\psi 4$ and $\Upsilon 4$ for pp collisions at 14 (red), 9.9 (blue), 7 (magenta) and 5.5 (green) TeV respectively.

The Quarkonium p_T Distribution in the $Q\overline{Q}$ NLO Code

Gaussian k_T smearing, $\langle k_T^2 \rangle_p = 1$ GeV^2 for fixed target pp and πp, broadened for pA and AA, NLO code adds in final state:

$$g_p(k_T) = \frac{1}{\pi \langle k_T^2 \rangle_p} \exp(-k_T^2/\langle k_T^2 \rangle_p)$$

Comparison with J/ψ and Υ Tevatron data at 1.8 TeV shows that the broadening should increase with energy, to $\langle k_T^2 \rangle_p \approx 2.5$ GeV^2

Fits of increase of $\langle p_T^2 \rangle$ to old data are inadequate to explain this increase so we make a simple linear extrapolation to obtain

$$\langle k_T^2 \rangle_p = 1 + \frac{1}{6} \ln \left(\frac{s}{s_0} \right) \text{ GeV}^2$$

Thus for pp collisions at LHC energies $\langle k_T^2 \rangle_p = 2.87$ GeV^2 for 5.5 TeV, 3.03 GeV^2 for 8.8 TeV and 3.18 GeV^2 for 14 TeV

Comparison with Tevatron Run I p_T Distributions

Agreement with trend of CDF Run I ($\sqrt{S} = 1.8$ TeV) is good overall

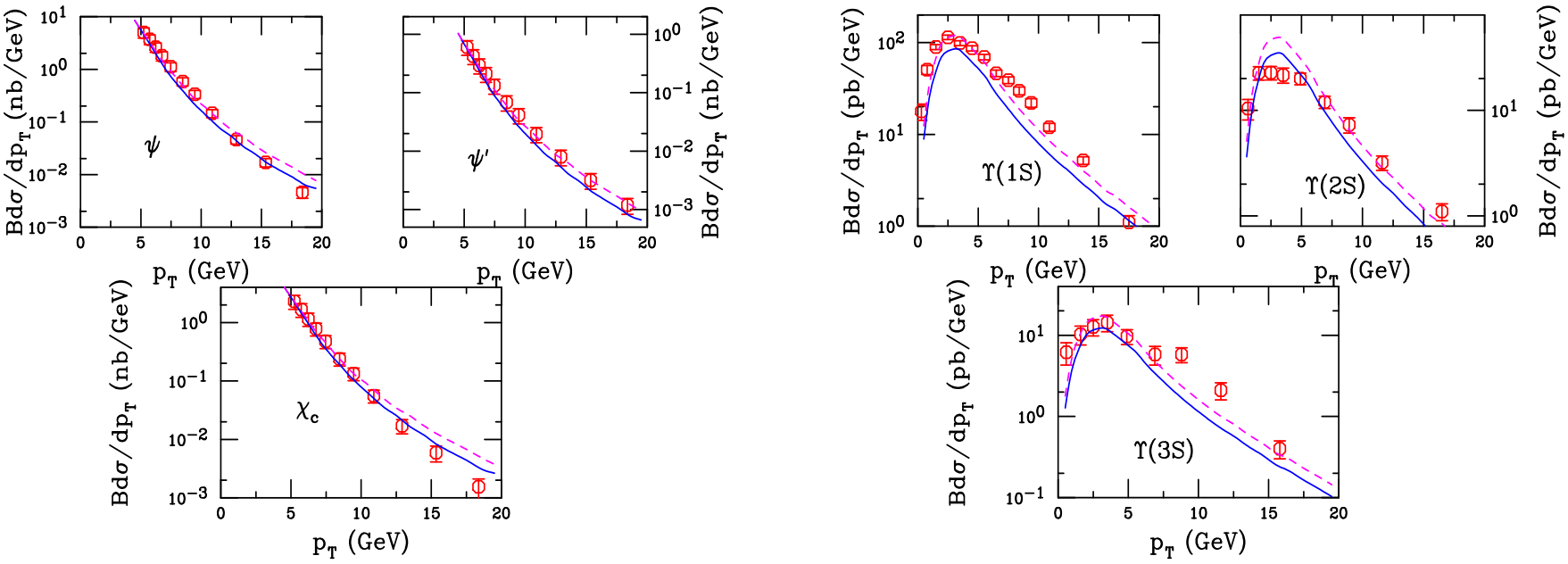

Figure 3: Left-hand side: The p_T distributions of direct J/ψ as well as J/ψ's from ψ' and χ_c decays calculated for MRST ($m_c = 1.2$ GeV, $\mu = 2m_T$) (solid) and GRV98 ($m_c = 1.3$ GeV, $\mu = m_T$) (dashed) are compared to the CDF data. We use $\langle k_T^2 \rangle_p = 2.5$ GeV^2. Right-hand side: The p_T distributions of inclusive $\Upsilon(1S)$, $\Upsilon(2S)$ and $\Upsilon(3S)$ calculated for MRST ($m_b = 4.75$ GeV and $\mu = m_T$) with $\langle k_T^2 \rangle_p = 3$ GeV^2 are compared to the CDF data. The dashed curve is multiplied by a K factor of 1.4.

Comparison with Tevatron Run II J/ψ p_T Distributions

Agreement with trend of CDF Run II ($\sqrt{S} = 1.96$ TeV) is good for $p_T > 2.5$ GeV

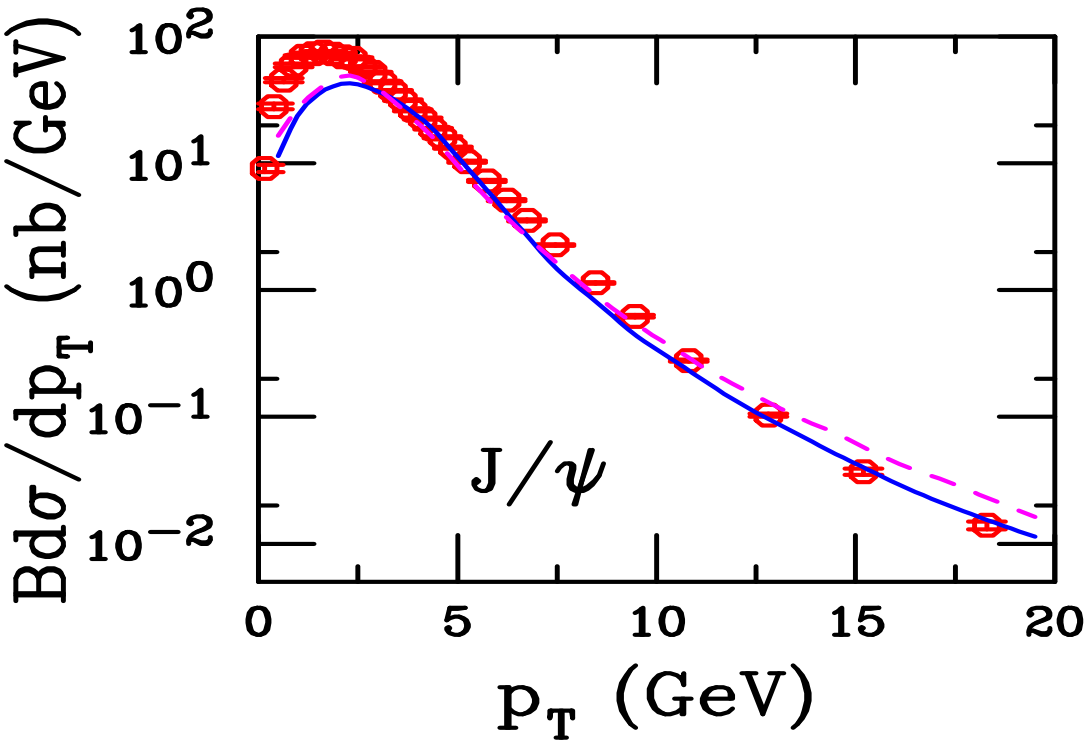

Figure 4: The inclusive J/ψ p_T distribution from Run II for MRST ($m_c = 1.2$ GeV, $\mu = 2m_T$) (solid) and GRV98 ($m_c = 1.3$ GeV, $\mu = m_T$) (dashed) are compared to the CDF data. We use $\langle k_T^2 \rangle_p = 2.5$ GeV^2.

Cold Nuclear Matter Effects

Nuclear effects in fixed-target interactions parameterized as

$$\sigma_{pA} = \sigma_{pp} A^{\alpha} \qquad \alpha(x_F, p_T)$$

$\sqrt{S_{NN}} \leq 40$ GeV and $x_F > 0.25$, α decreases strongly with x_F – only low x_F effects probed by SPS and collider rapidity coverage

Two low x_F cold matter effects on the total rate at colliders:

- **Nuclear Shadowing — initial-state effect on the PDFs affecting total rate as a function of y/x_F, increases with A, $\sqrt{S}$**
- **Nucleon absorption — final-state effect on produced $Q\overline{Q}$, independent of y in acceptance of collider detectors, increases with A, decreases with $\sqrt{S}$ (Braun *et al.*, Capella and Ferreiro), consistent with SPS (in antishadowing range, implies larger 'absorption' cross section than absorption alone) to RHIC observations**

At $x_F > 0.25$, other mechanisms (energy loss, intrinsic charm) may be important but this corresponds to $y > 6$ at $\sqrt{S_{NN}} = 5.5$ TeV, out of range of measurement

Comparing Shadowing Parameterizations: x Dependence

EKS98 and nDSg, agree best with RHIC d+Au, available for all A

EKS98 has strong antishadowing at $x \sim 0.1$, nDSg has almost none

EKS98 and nDSg similar for $A = 208$ but nDSg weaker for smaller A

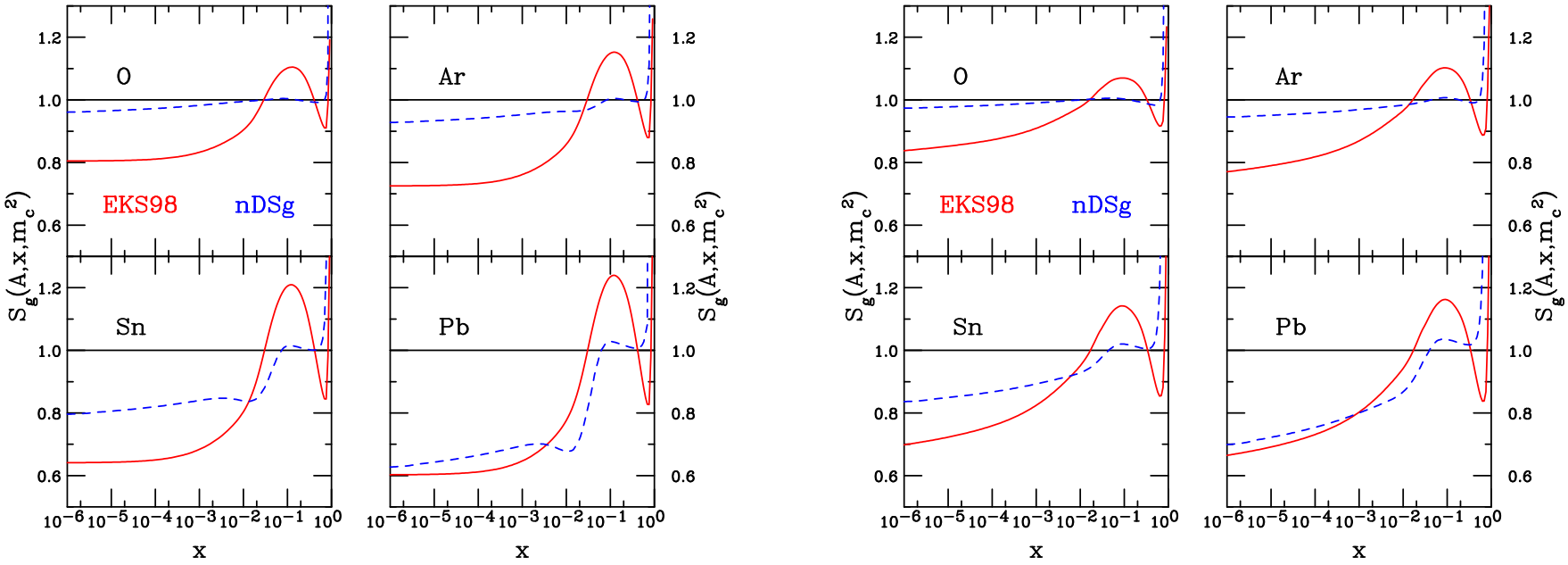

Figure 5: EKS98 (red) and nDSg (blue) gluon shadowing parameterizations for J/ψ (left) and Υ (right) production scales for A =O, Ar, Sn and Pb.

Average x_2 as a Function of Energy and Rapidity

$\langle x_2 \rangle$ as a function of rapidity for $2 \to 2$ scattering (N.B. $\langle x_1 \rangle$ is mirror imagine of $\langle x_2 \rangle$)

Increasing $\sqrt{S}$ broadens y range and decreases x_2

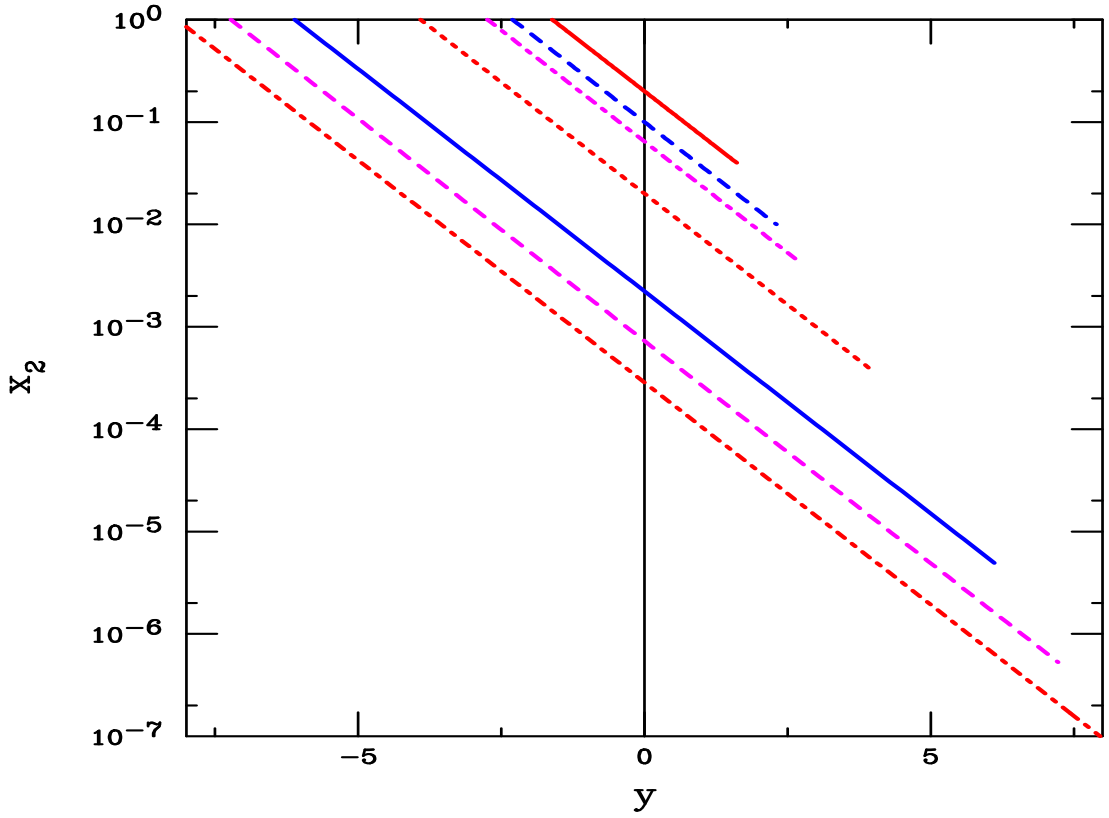

Figure 6: We give the average value of the nucleon momentum fraction, x_2, in pp collisions as a function of rapidity for (top to bottom) $\sqrt{S_{NN}} = 20$; 40; 62; 200; 1800; 5500 and 14000 GeV.

Predicted J/ψ Rapidity Distributions at RHIC

Agreement of color evaporation model (CEM) with overall normalization of PHENIX data good

Shape has right trend for d+Au with EKS98 shadowing

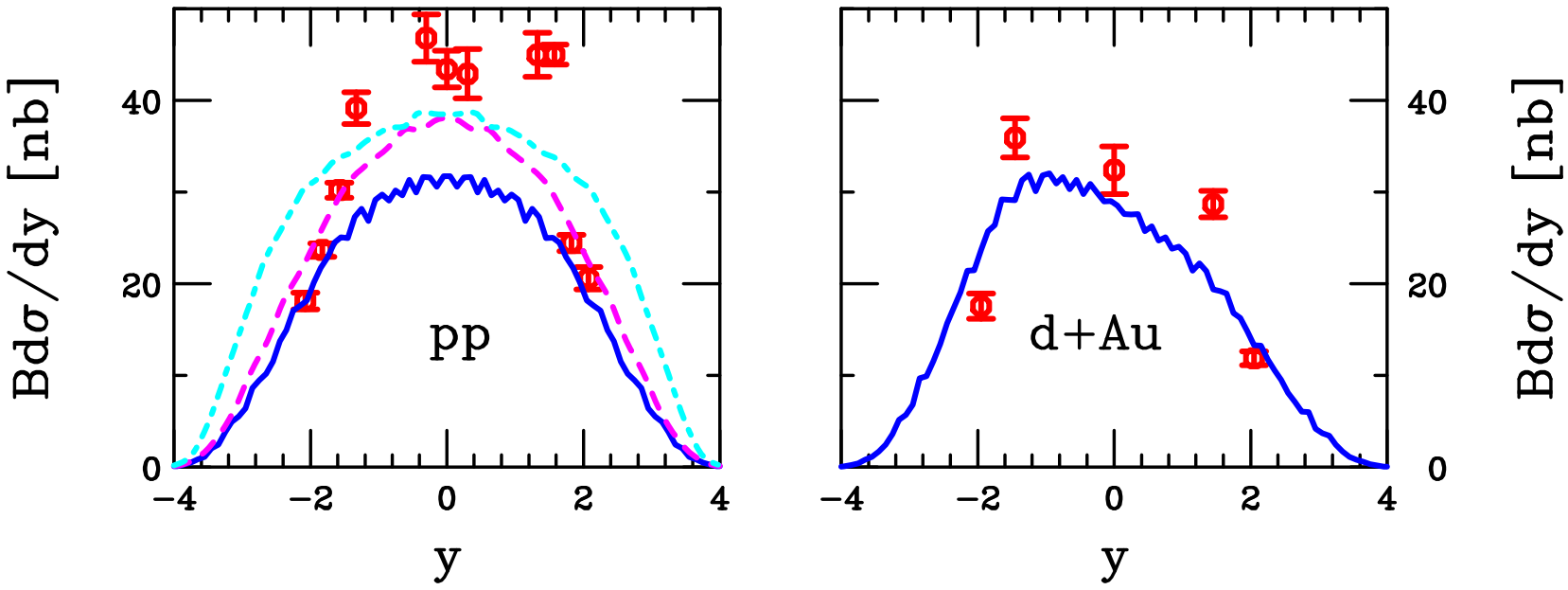

Figure 7: The inclusive J/ψ y distributions in $\sqrt{S} = 200$ GeV pp interactions (left-hand side) calculated with the MRST parton densities in the CEM with $m_c = 1.2$ GeV, $\mu = 2m_T$. The rapidity distribution for d+Au collisions (right-hand side with EKS98) is also shown.

Absorption and Shadowing at RHIC: $R_{\rm dAu}(y)$

Feeddown from higher states with larger absorption cross sections needs $\sigma_{\rm abs}^{J/\psi} < 2$ mb with present d+Au data

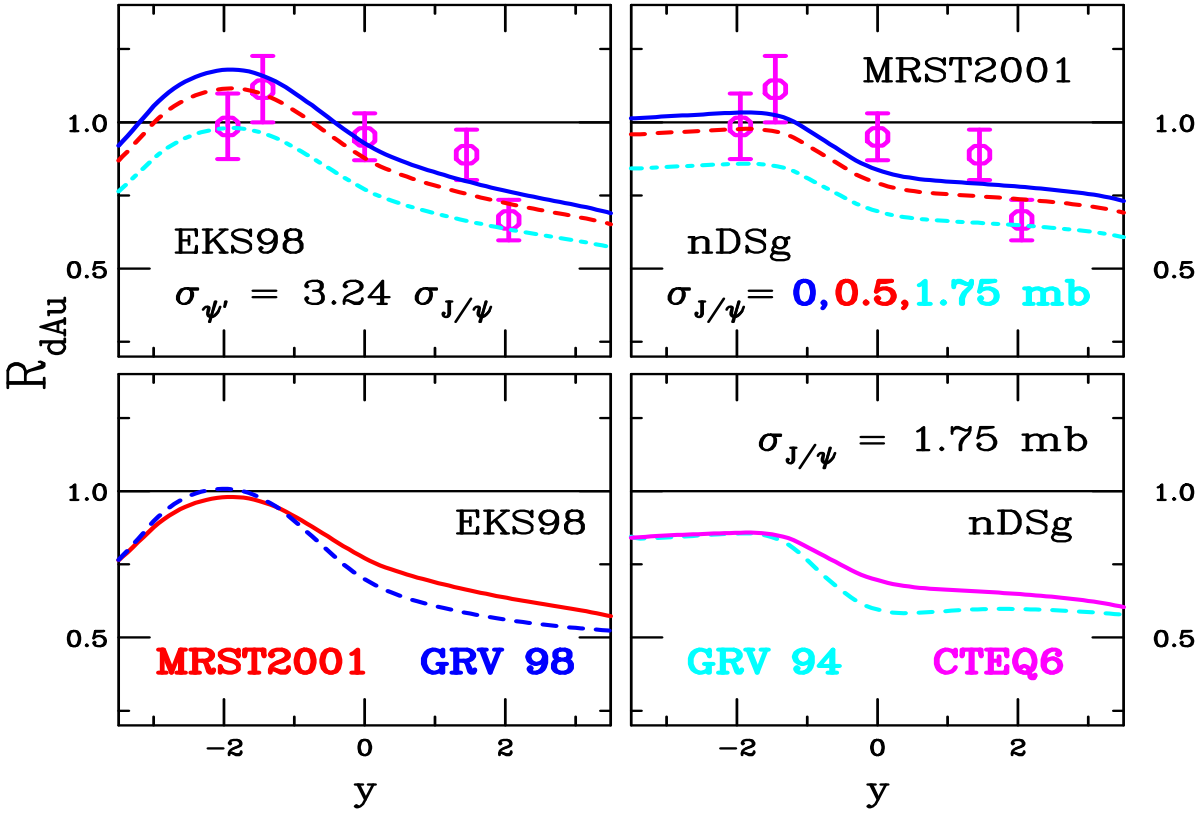

Figure 8: The d+Au/*pp* minimum bias ratio as a function of rapidity for EKS98 (left) and nDSg (right) parameterizations. The top plots vary the J/ψ absorption cross section with the MRST2001 PDFs while the bottom plots show the differences in the PDF choice for a fixed absorption cross section.

Absorption and Shadowing at RHIC: $R_{\rm dAu}(N_{\rm coll})$

Largest difference between shadowing parameterizations is in anti-shadowing region ($y = -1.7$), PDF difference is not large

Data do not strongly distinguish between different $\sigma_{\rm abs}$

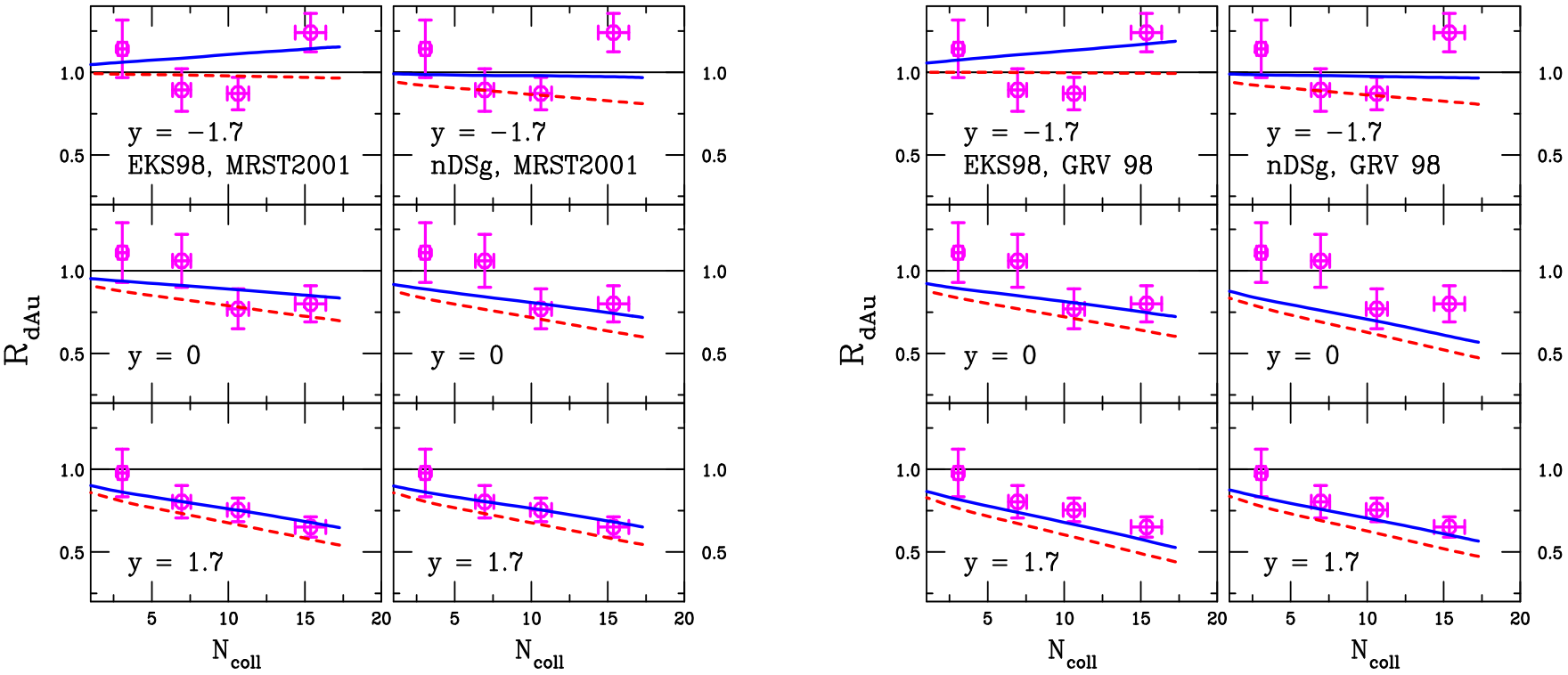

Figure 9: The dAu/pp ratio as a function of the number of collisions calculated with EKS98 (left) and nDSg (right) on each plot with the MRST2001 (left-hand plot) and GRV 98 (right-hand plot) PDFs. The curves are for $\sigma_{\rm abs}^{J/\psi} = 0.5$ (solid blue) and 1.75 mb (dashed red). PHENIX data are shown for d+Au collisions at 200 GeV for $y = -1.7$ (top), 0 (middle) and 1.7 (bottom). (An additional 12% overall normalization error is not shown.)

Absorption and Shadowing at RHIC: $R_{\rm AuAu}(y)$

R_{AA} rather flat with rapidity, agreement with data for $\sigma_{\rm abs}^{J/\psi} \sim 1$ mb

Convolution of shadowing parameterizations give dip at midrapidity

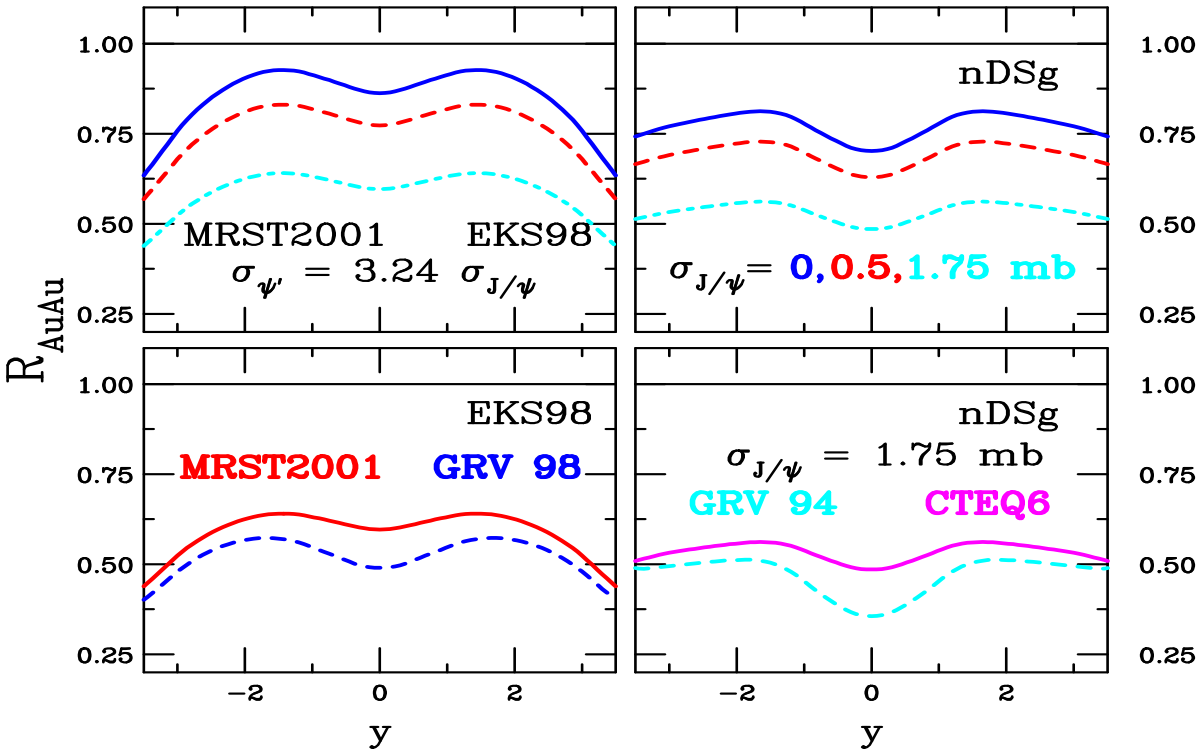

Figure 10: The AuAu/pp minimum bias ratio as a function of rapidity for EKS98 (left) and nDSg (right) parameterizations. The top plots vary the J/ψ absorption cross section with the MRST2001 PDFs while the bottom plots show the differences in the PDF choice for a fixed absorption cross section.

Why is $R_{\rm AuAu}(y)$ higher at $y = 2$?

$R_{\rm dAu}$ is lower at $y = 2$ than at $y = 0$ but $R_{\rm AuAu}$ is not

Cyan curve is $R_{\rm Aud}$, multiply blue times cyan curves at each y and get magenta curve, including absorption moves all curves down

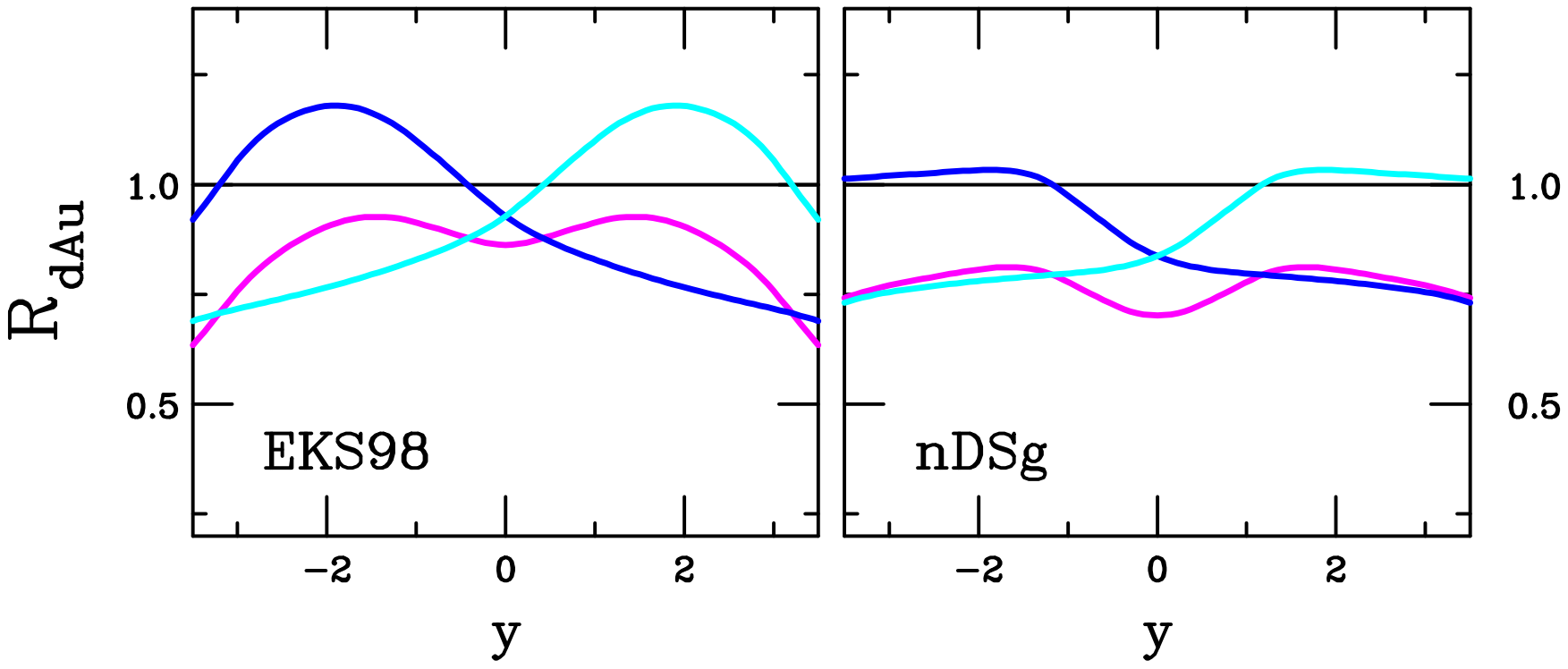

Figure 11: The dAu/*pp* (blue), Aud/*pp* (cyan) and AuAu/*pp* (magenta) ratios as a function of rapidity for EKS98 (left) and nDSg (right) parameterizations with the MRST2001 PDFs.

How to get $R_{\rm AuAu}(y=2)/R_{\rm AuAu}(y=0)<1$

Reduce gluon antishadowing so that $R_{\rm dAu}\approx 1$ at $y=0$ and shadowing at higher y

This would also require modifying quark shadowing and satisfying momentum sum rule – no parameterization gives this shape – nDSg comes close but shadowing comes before $y=0$ and still gives dip at $y=0$

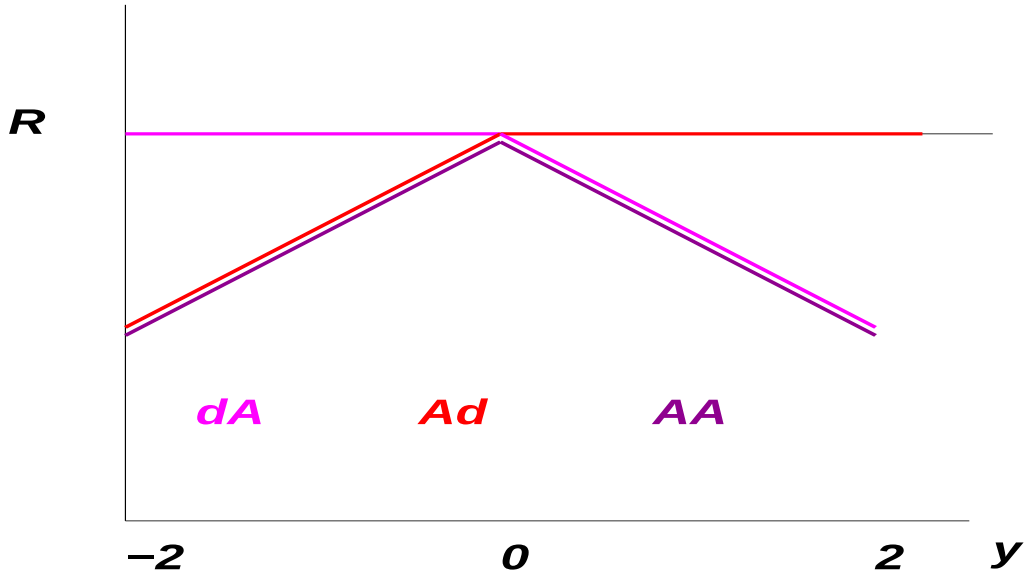

Figure 12: The dAu/pp (magenta), Aud/pp (red) and AuAu/pp (purple) ratios as a function of rapidity to make $R_{AA}(y=2)/R_{AA}(y=0)<1$

Absorption and Shadowing at RHIC: $R_{\rm AuAu}(N_{\rm part})$

Cold matter effects with $\sigma_{\rm abs} \sim 1$ mb in relatively good agreement with midrapidity data

Stronger $N_{\rm part}$ dependence at forward rapidity than predicted

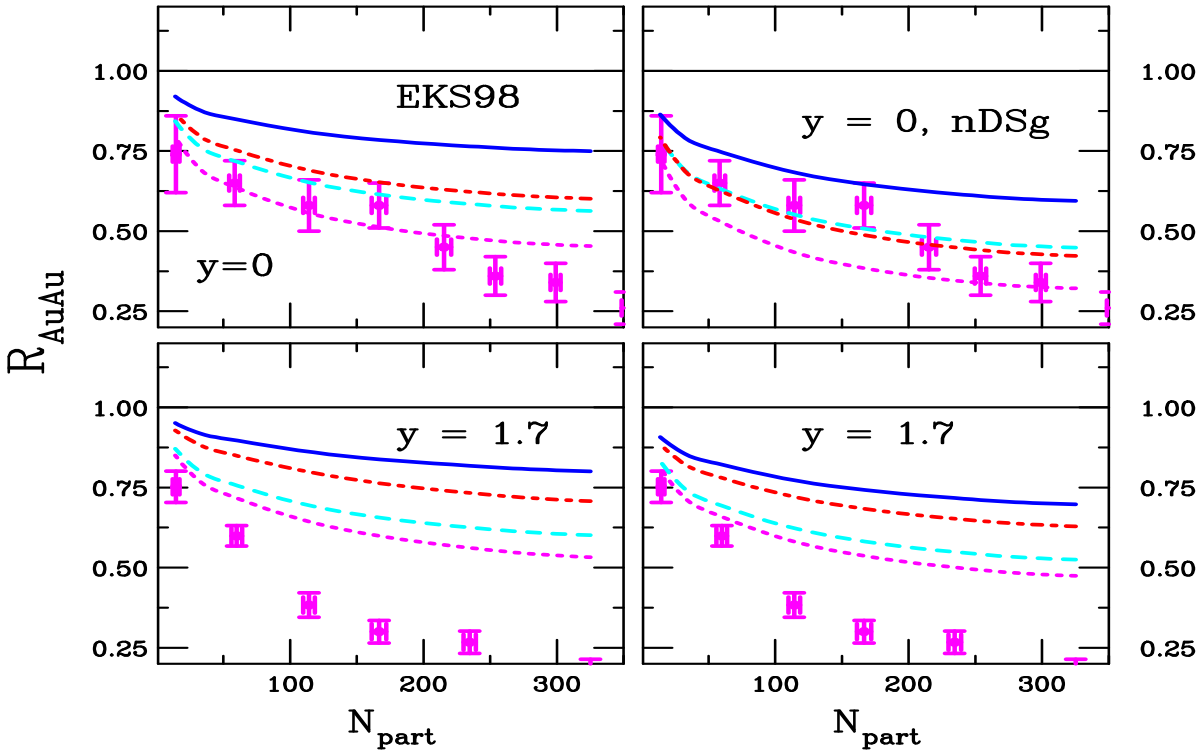

Figure 13: The AuAu/pp ratio as a function of the number of participants calculated with EKS98 (left) and nDSg (right). The curves are for $\sigma_{\rm abs}^{J/\psi} = 0.5$ (solid blue - MRST2001 and dot-dashed red - GRV 98) and 1.75 mb (dashed cyan - MRST2001 and dotted magenta - GRV 98). PHENIX data are shown for Au+Au collisions at 200 GeV for $y = 0$ (top), and 1.7 (bottom).

Absorption and Shadowing at RHIC: Centrality Dependence of $R_{\rm AuAu}(y)$, GRV 98

Shadowing considerably reduced in peripheral Au+Au, b dependence of absorption also taken into account

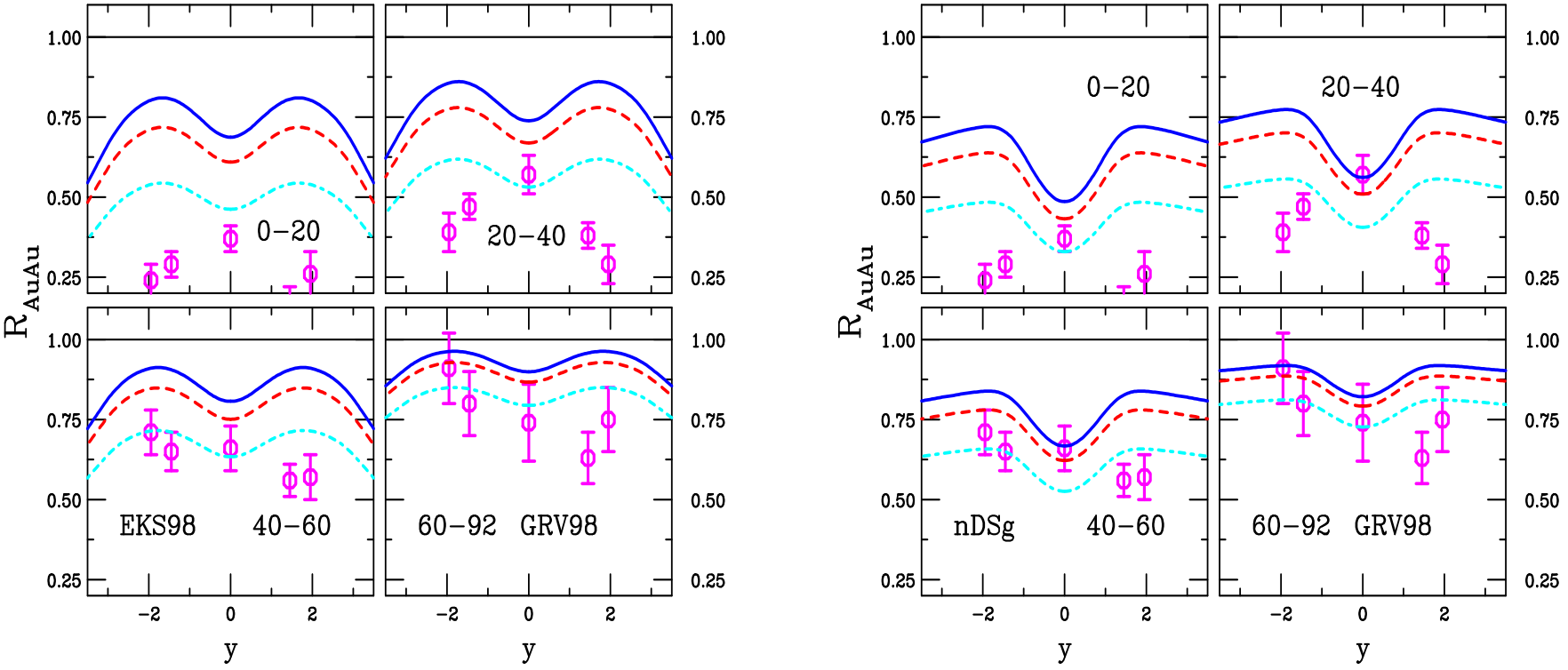

Figure 14: The AuAu/pp ratio as a function of y in the four PHENIX centrality bins compared to the data. The calculations with the GRV98 PDFs are shown with EKS98 (left-hand plot) and nDSg (right-hand plot). The curves are for $\sigma_{\rm abs}^{J/\psi} = 0$ (solid blue), 0.5 mb (dashed red) and 1.75 mb (dot-dashed cyan).

Absorption and Shadowing at RHIC: Centrality Dependence of $R_{\rm AuAu}(y)$, MRST2001

Larger scale with MRST2001 PDFs gives somewhat weaker shadowing effect

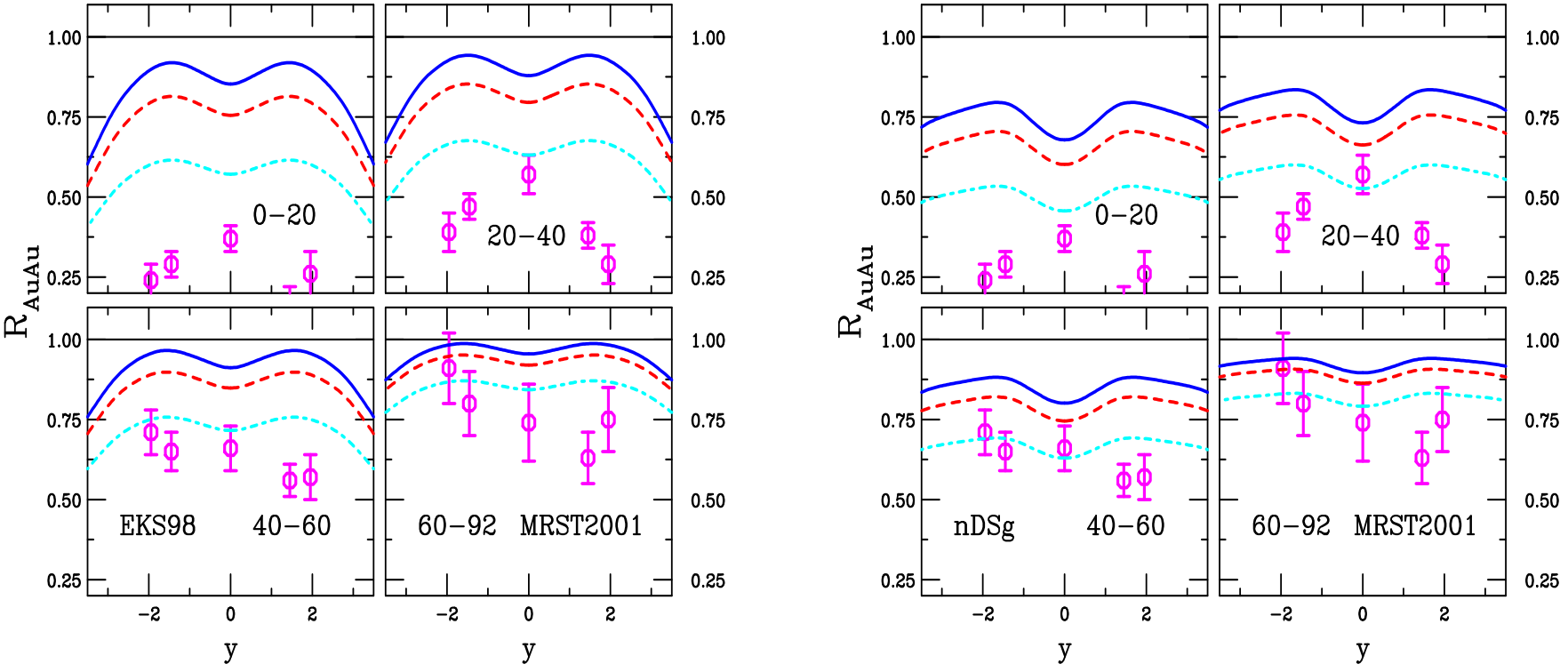

Figure 15: The AuAu/pp ratio as a function of y in the four PHENIX centrality bins compared to the data. The calculations with the MRST2001 PDFs are shown with EKS98 (left-hand plot) and nDSg (right-hand plot). The curves are for $\sigma_{\rm abs}^{J/\psi} = 0$ (solid blue), 0.5 mb (dashed red) and 1.75 mb (dot-dashed cyan).

Shadowing in pA at the LHC

Includes more realistic ratios with respect to pp at 14 TeV and pA rapidity shift, no absorption

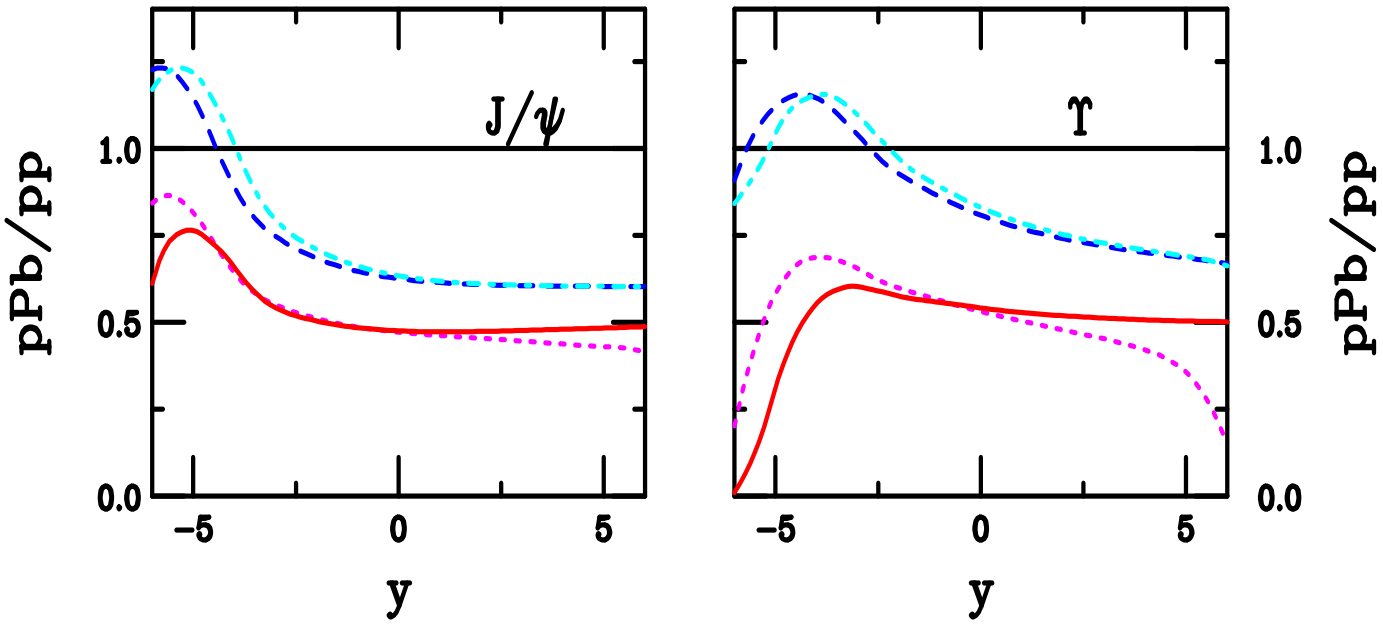

Figure 16: The J/ψ (left) and Υ (right) pPb/pp ratios as a function of rapidity. The pPb/pp ratios are given for 8.8 (dashed) and 5.5 (dot-dashed) TeV collisions in both cases and 8.8 TeV pPb to 14 TeV pp without (dotted) and with (solid) the beam rapidity shift taken into account. The Pb beam comes from the right.

Shadowing in Pb+Pb at the LHC

Includes more realistic ratios with respect to pp at 14 TeV, little difference in EKS98 and nDSg results

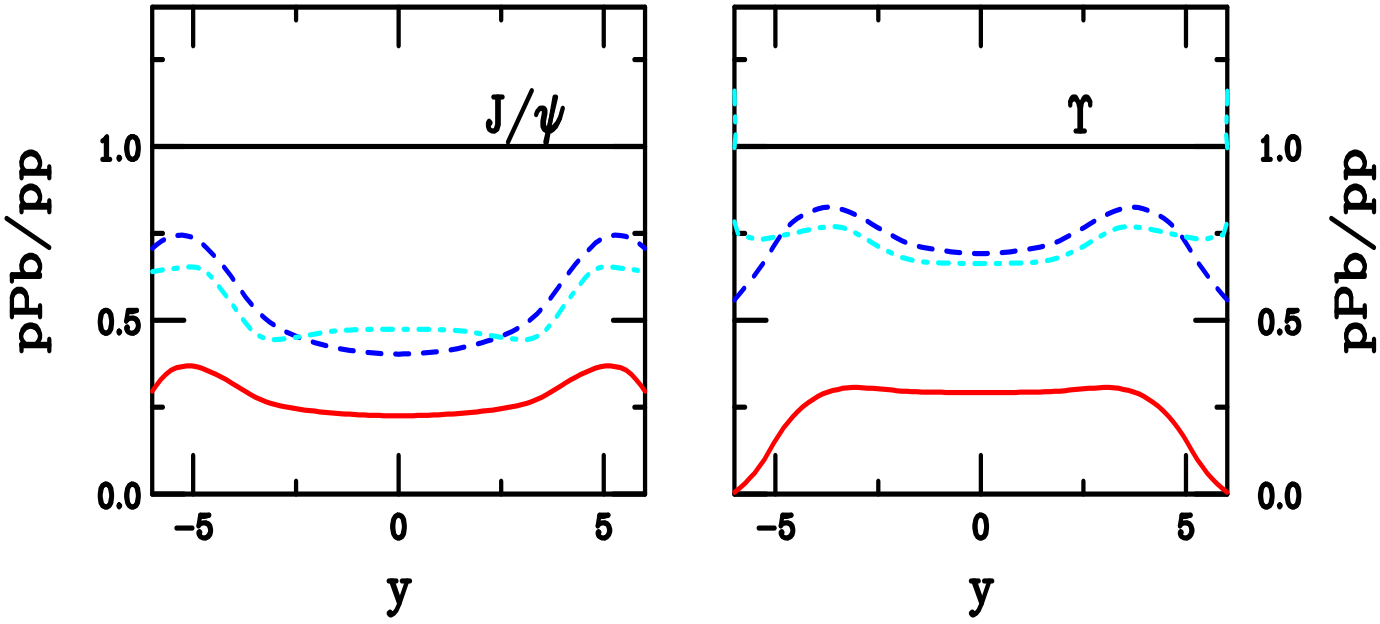

Figure 17: The J/ψ (left) and Υ (right) PbPb/pp ratios as a function of rapidity. The PbPb/pp ratios are shown for 5.5 TeV in both cases with EKS98 (dashed) and nDSg (dot-dashed) shadowing and also for 5.5 TeV Pb+Pb and 14 TeV pp (solid).

Inhomogeneous Quarkonium Shadowing and Absorption

LHC Pb+Pb results presented as a function of $N_{\rm coll}$ for several rapidities: 0, 2 and 4 for EKS98 and nDSg parameterizations

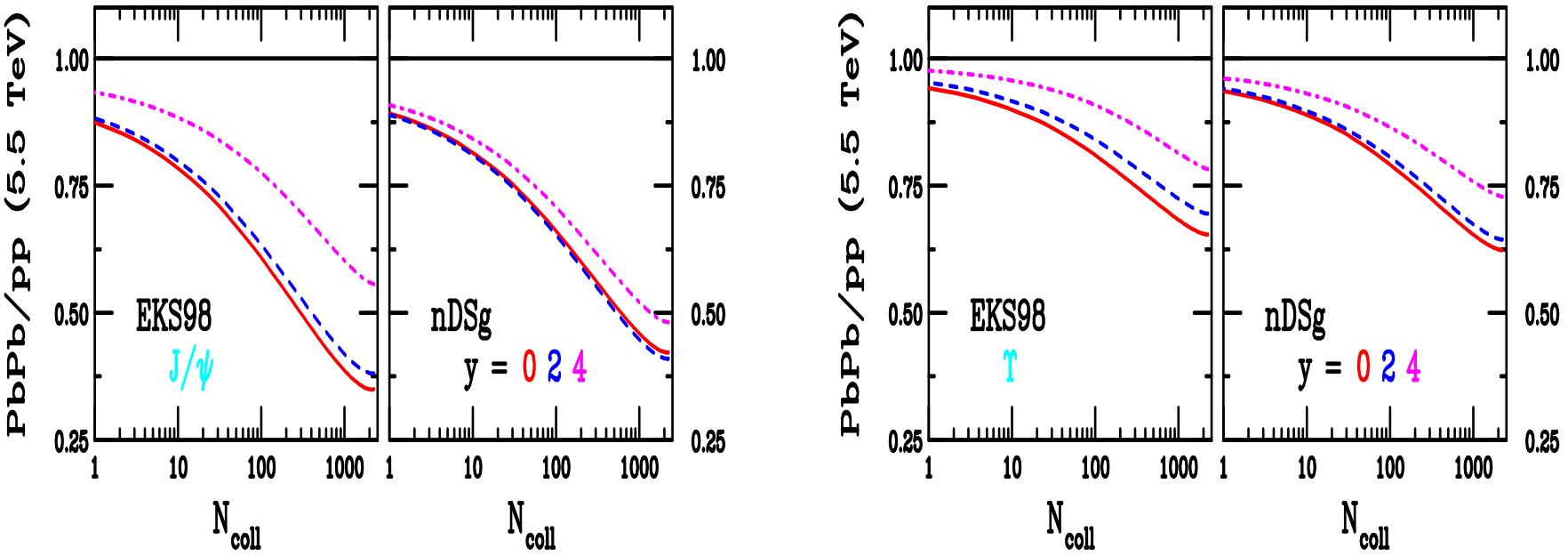

Figure 18: The J/ψ (left-hand side) and Υ (right-hand side) Pb+Pb/pp ratio as a function of $N_{\rm coll}$. The results are shown at $y = 0$ (solid), 2 (dashed) and 4 (dot-dashed). The EKS98 (left) and nDSg (right) parameterizations are compared.

Quarkonium Suppression by Color Screening

Matsui and Satz predicted J/ψ suppression

'Normal absorption' observed in pA, $\sigma_{pA} = \sigma_{pp} A^{\alpha}$ (NA3, E537, E866, NA50, HERA-B)

'Normal' includes all cold nuclear matter effects: nucleon absorption, any comover scattering, nuclear shadowing, energy loss, all are wrapped up in α

AA data at SPS (high E_T) and RHIC (high $N_{\rm part}$) exhibit stronger than 'normal' absorption

Central RHIC data may be consistent with some $c\bar{c}$ coalescence, should be larger effect at the LHC

$\Upsilon(1S)$ state is small, breakup by screening more difficult, good probe for LHC

Simple Estimate of Maximum p_T For Suppression

Formation time of quarkonium states in lab

$$t_F = \tau_F \sqrt{1 + (p_T/M)^2}$$

Time system center remains above T_c, assuming isentropic expansion

$$\begin{aligned} s_D t_D(0) &= s_0 t_0 \\ t_D(0) &= t_0 \left(\frac{T_0}{T_c}\right)^3 \end{aligned}$$

Suppression occurs for $t_D(0)/t_F > 1$, corresponding to maximum p_T

$$p_{T\,\mathrm{m}} = M\sqrt{(t_D(0)/\tau_F)^2 - 1}$$

Maximum effective screening p_T may be less than $p_{T\,\mathrm{m}}$ due to finite system size

Survival Probability vs. p_T

Suppression pattern depends on initial conditions, system size, τ_F, and M

From entropy profile: $t_D(r) = t_D(0)(1-(r/R)^2)^{1/4}$, $R \leq R_{\rm Pb}$

Boundary of screening region: $r_S = R(1-(t/t_D(0))^{1/4})^{1/2}$

$Q\overline{Q}$ pair produced at $x^\mu = (0, \vec{r}, 0)$, $p^\mu = (\sqrt{M^2+p_T^2}, \vec{p}_T, 0)$

Quarkonium state formed at $x^\mu = (\tau_F\sqrt{1+(p_T/M)^2}, \vec{r}+\tau_F\vec{p}_T/M, 0)$

State survives if $|\vec{r}+\tau_F\vec{p}_T/M| \geq r_S$

$$
\begin{aligned}
S(p_T) &= \frac{\int_0^R dr r\rho(r)\theta_(r,p_T)}{\pi\int_0^R dr r\rho(r)} \\
\rho(r) &= (1-(r/R)^2)^{1/2} \\
\theta(r,p_T) &= \begin{cases} \pi & z \leq -1 \quad \textbf{always survives} \\ \cos^{-1} z & |z|<1 \quad \textbf{sometimes survives} \\ 0 & z \geq 1 \quad \textbf{never survives} \end{cases} \\
z &= \frac{r_S^2 - r^2 - (\tau_F p_T/M)^2}{2r\tau_F p_T/M}
\end{aligned}
$$

Studying QGP Characteristics via Quarkonium p_T Ratios

The ψ'/ψ and Υ'/Υ ratios are independent of p_T at the Tevatron (similar to color evaporation model predictions)

Effects of cold nuclear medium should be similar for ψ and ψ' and also for Υ, Υ' and Υ'': similar A dependence for each quarkonium type, especially if absorption is negligible at LHC energies

No difference in shadowing effects expected for quarkonium states of the same family for color evaporation model (same x) but may be some small effect due to different singlet/octet production ratios for nonrelativistic QCD

Thus only QGP effects can significantly affect the p_T dependence of the ratios

$Q\overline{Q}$ coalescence will be strongest at low p_T, unclear how it affects p_T dependence of ψ'/ψ and Υ'/Υ, should be smaller effect on Υ states

Strongly dependent on initial conditions (Gunion and Vogt) – updated here with newer screening calculations

Initial Conditions and Screening Scenarios

Initial time and temperature of QGP at the LHC: $\tau_0 = 0.2$ **fm and** $700 < T_0 < 850$ **MeV (Vitev),** $T_c = 173$ **MeV from lattice**

Assume two scenarios for quarkonium screening:

- **Digal, Petreczky and Satz:** $\mu = 1.15T$**, screening on Coulomb potential only, rather low dissociation temperatures –** $1.1T_c$ **for the** J/ψ **and** $2.3T_c$ **for the** Υ **(**χ_c**,** ψ'**,** Υ'' **and** $\chi_c(2P)$ **dissociate at** $T < T_c$**)**
- **Satz:** $\mu = 1.45T$ **for** $T > 1.1T_c$ **(newer evaluation), screening on the Coulomb and linear terms, higher dissociation temperatures –** $2.1T_c$ **for the** J/ψ **and** $4.1T_c$ **for the** Υ**, no states break up below** T_c**, in better agreement with lattice spectral function calculations**

	T_D/T_c							
μ/T	J/ψ	χ_c	ψ'	Υ	$\chi_b(1P)$	Υ'	$\chi_b(2P)$	Υ''
1.15	**1.10**	**0.74**	**0.10–0.20**	**2.31**	**1.13**	**1.10**	**0.83**	**0.75**
1.45	**2.10**	**1.16**	**1.12**	**4.10**	**1.76**	**1.60**	**1.19**	**1.17**

Table 1: The quarkonium dissociation temperatures for the two scenarios above.

Quarkonium survival probability vs. p_T

$S(p_T)$ very sensitive to initial conditions, screening scenario

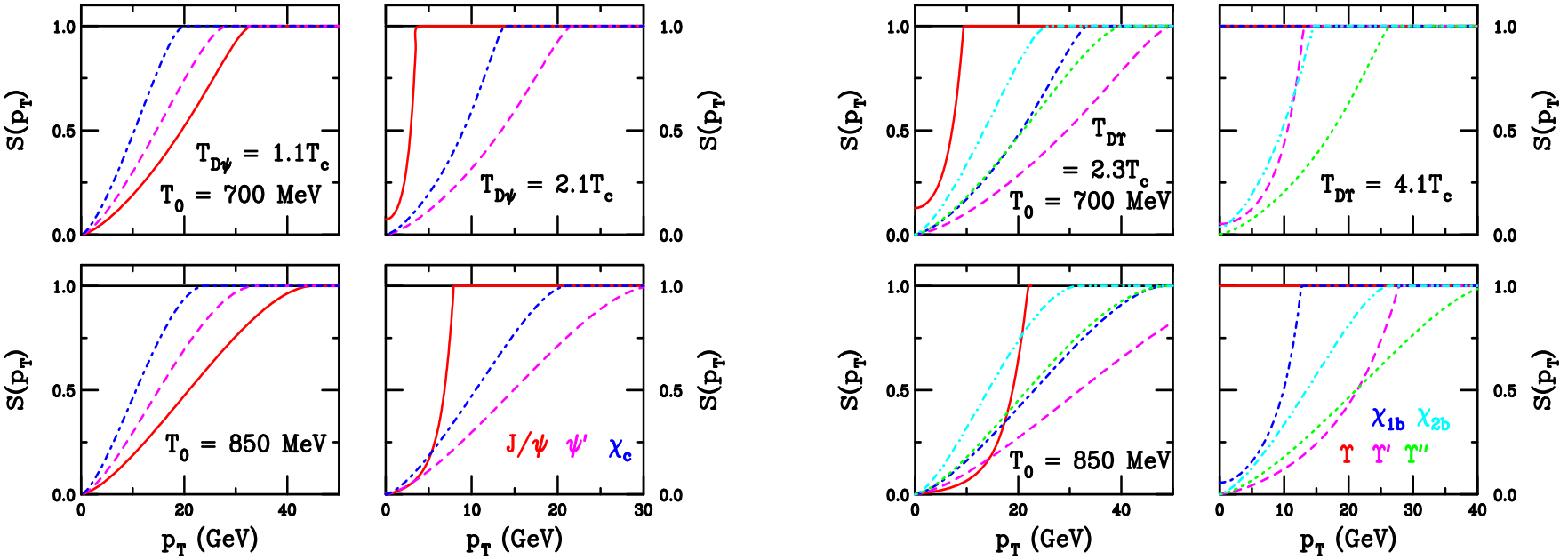

Figure 19: The survival probabilities as a function of p_T for the charmonium (left-hand side) and bottomonium (right-hand side) states for initial conditions at the LHC. The charmonium survival probabilities are J/ψ (solid), χ_c (dot-dashed) and ψ' (dashed) respectively. The bottomonium survival probabilities are given for Υ (solid), χ_{1b} (dot-dashed), Υ' (dashed), χ_{2b} (dot-dot-dash-dashed) and Υ'' (dotted) respectively. The top plots are for $T_0 = 700$ MeV while the bottom are for $T_0 = 850$ MeV. The left-hand sides of the plots for each state are for the lower dissociation temperatures, $1.1T_c$ for the J/ψ and $2.3T_c$ for the Υ while the right-hand sides show the results for the higher dissociation temperatures, $2.1T_c$ for the J/ψ and $4.1T_c$ for the Υ.

Direct Suppression Ratios vs. p_T

Assuming direct production can be separated

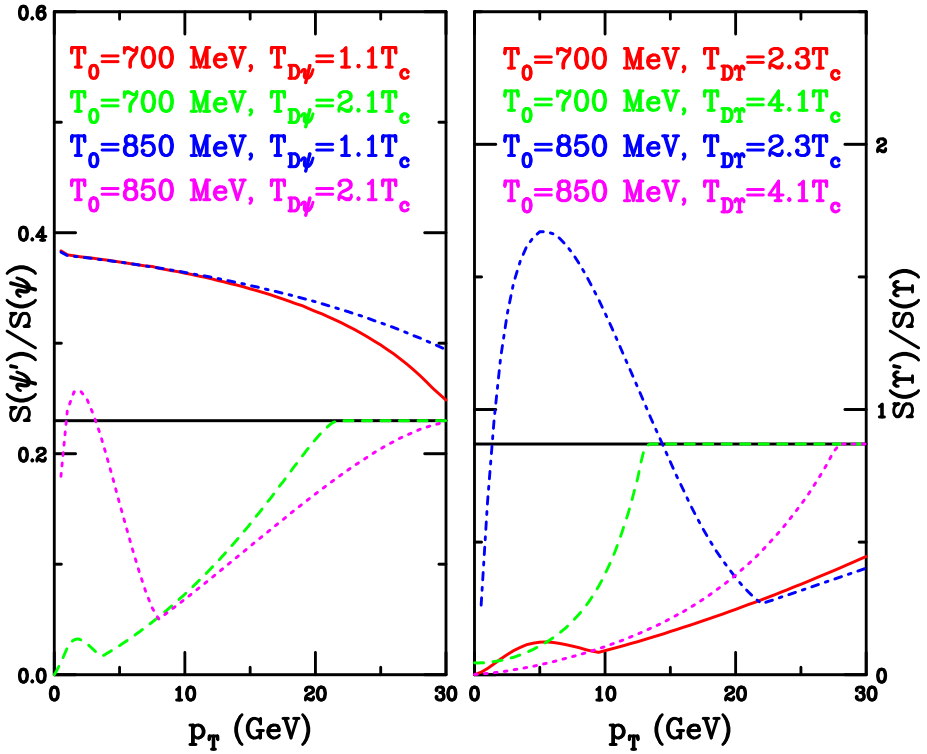

Figure 20: The direct ψ'/ψ (left) and Υ'/Υ (right) ratios as a function of p_T in Pb+Pb collisions at 5.5 TeV for $T_0 = 700$ MeV (solid and dashed) and 850 MeV (dot-dashed and dotted). The ψ (Υ) results are shown for assumed dissociation temperatures of $1.1T_c$ ($2.3T_c$) (solid and dot-dashed) and $2.1T_c$ ($4.1T_c$) (dashed and dotted) respectively.

Indirect Suppression Ratios vs. p_T

Including feed down from higher states, no coalescence effects included

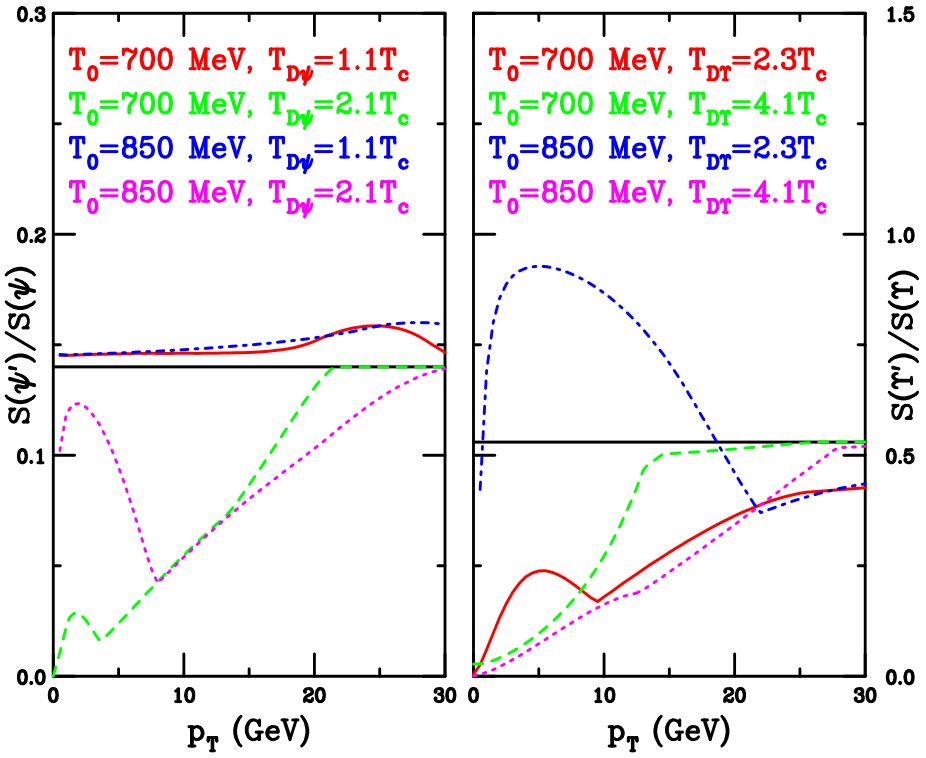

Figure 21: The indirect ψ'/ψ (left) and Υ'/Υ (right) ratios as a function of p_T in Pb+Pb collisions at 5.5 TeV for $T_0 = 700$ MeV (solid and dashed) and 850 MeV (dot-dashed and dotted). The ψ (Υ) results are shown for assumed dissociation temperatures of $1.1T_c$ ($2.3T_c$) (solid and dot-dashed) and $2.1T_c$ ($4.1T_c$) (dashed and dotted) respectively.

Summary .

- Results only shown for inclusive J/ψ and Υ but pp and pA measurements of χ_c, ψ', χ_b, Υ' and Υ'' should be possible at the LHC with similar pp distributions, χ absorption should be different – check production and absorption mechanisms
- Nuclear modification in d+Au relative to pp interactions at 200 GeV consistent with predictions of nuclear shadowing parameterizations with small absorption by nucleons
- Comparison to pp at 14 TeV instead of pp at the same energy does not wash out shadowing and absorption effects
- pA interactions at more than one A may be necessary to distinguish between shadowing models
- High LHC energies provide exciting opportunity to measure low x parton densities at moderate to high Q^2
- Quarkonium p_T ratios should be able to distinguish between plasma models and initial conditions